Li^+ Cation Environment, Transport, and Mechanical Properties of the LiTFSI Doped *N*-Methyl-*N*-alkylpyrrolidinium$^+$TFSI$^-$ Ionic Liquids

Oleg Borodin,*,† Grant D. Smith,†,‡ and Wesley Henderson§

Department of Materials Science & Engineering, 122 S. Central Campus Drive, Rm 304, University of Utah, Salt Lake City, Utah 84112-0560, Department of Chemical Engineering, University of Utah, Salt Lake City, Utah 84112-0560, and Department of Chemistry, U.S. Naval Academy, 572 M Holloway Road, Annapolis, Maryland 21402

Received: March 28, 2006; In Final Form: May 25, 2006

Molecular dynamics (MD) simulations have been performed on *N*-methyl-*N*-propylpyrrolidinium bis(trifluoromethanesulfonyl)imide (mppy$^+$TFSI$^-$) and *N*,*N*-dimethyl- pyrrolidinium bis(trifluoromethanesulfonyl)imide (mmpy$^+$TFSI$^+$) ionic liquids (ILs) doped with 0.25 mol fraction LiTFSI salt at 303−500 K. The liquid density, ion self-diffusion coefficients, and conductivity predicted by MD simulations were found to be in good agreement with experimental data, where available. MD simulations reveal that the Li^+ environment is similar in mppy$^+$TFSI$^-$ and mmpy$^+$TFSI$^+$ ILs doped with LiTFSI. The Li^+ cations were found to be coordinated on average by slightly less than four oxygen atoms with each oxygen atom being contributed by a different TFSI$^-$ anion. Significant lithium aggregation by sharing up to three TFSI$^-$ anions bridging two lithiums was observed, particularly at lower temperatures where the lithium aggregates were found to be stable for tens of nanoseconds. Polarization of TFSI$^-$ anions is largely responsible for the formation of such lithium aggregates. Li^+ transport was found to occur primarily by exchange of TFSI$^-$ anions in the first coordination shell with a smaller (∼30%) contribution also due to Li^+ cations diffusing together with their first coordination shell. In both ILs, ion self-diffusion coefficients followed the order Li^+ < TFSI$^-$ < mmpy$^+$ or mppy$^+$ with all ion diffusion in mmpy$^+$TFSI$^-$ being systematically slower than that in mppy$^+$TFSI$^-$. Conductivity due to the Li^+ cation in LiTFSI doped mppy$^+$TFSI$^-$ IL was found to be greater than that for a model poly(ethylene oxide)-(PEO)/LiTFSI polymer electrolyte but significantly lower than that for an ethylene carbonate/LiTFSI liquid electrolyte. Finally, the time-dependent shear modulus for the LiTFSI doped ILs was found to be similar to that for a model poly(ethylene oxide)(PEO)/LiTFSI polymer electrolyte on the subnanosecond time scale.

I. Introduction

The ability of ionic liquids (ILs) to dissolve lithium salts and transport Li^+ cations positions them as competitors with liquid, gel, and polymer electrolytes for applications in lithium batteries. The negligible vapor pressure, high thermal and electrochemical stability, and better Li^+ transport properties of ILs relative to polymer electrolytes yields an excellent combination of favorable electrolyte transport properties and safety characteristics.[1] Moreover, ILs doped with lithium salts may be dissolved in polymers resulting in flexible membranes with excellent mechanical properties, exceptional electrochemical stability, and good Li^+ transport.[2,3]

The structure and ion transport properties of a number of ILs (primarily imidazolium-based) are well understood as a result of hundreds of experimental studies and tens of molecular dynamics simulations reported in recent years. The Li^+ cation environment and its transport mechanism in lithium salt doped ILs, however, has been studied much less intensively experimentally,[1−3,4,5] and no molecular dynamics (MD) simulations of lithium salt doped ILs have been reported to the best of our knowledge. MD simulations are well suited for exploring structure and transport in lithium salt doped ILs since ions move sufficiently far on the time scales accessible to MD simulations (multiple nanoseconds) to permit the determination of transport properties and equilibrium structure.

In our previous work,[6−10] we developed and validated force fields for *N*-alkyl-*N*-methylpyrrolidinium cations,[6] bis(trifluoromethanesulfonyl)imide (TFSI$^-$) anions including TFSI$^-$ interactions with Li^+, and various liquid and polymer solvents. In this paper, we extend our study to examine pyrrolidinium$^+$TFSI$^-$ ILs doped with LiTFSI focusing on the Li^+ environment and its transport mechanisms. We selected two electrolytes for the molecular dynamics (MD) simulations study: a mixture of 0.25 mole fraction LiTFSI with 0.75 mole fraction *N*,*N*-dimethylpyrrolidinium$^+$TFSI$^-$ (mmpy$^+$TFSI$^-$) denoted as 0.25 LiTFSI−0.75 mppy$^+$TFSI$^-$, and a mixture of 0.25 mole fraction LiTFSI with 0.75 *N*,*N*-dimethylpyrrolidinium$^+$-TFSI$^-$ (0.25 LiTFSI−0.75 mmpy$^+$TFSI$^-$). The mmpy$^+$ and mppy$^+$ cations and TFSI$^-$ anion are illustrated in Figure 1. Conductivity, density, self-diffusion coefficients, and phase diagrams of these mixtures have been recently reported.[11,12] The 0.25 LiTFSI−0.75 mppy$^+$TFSI$^-$ and 0.25 LiTFSI−0.75 mmpy$^+$TFSI$^-$ electrolytes were found to be in a liquid state at temperatures above about 30 and 60 °C, respectively,[11,13] and possess sufficient conductivity >0.1 mS/cm in the liquid state to allow ion transport to be observed in MD simulations on a nanosecond time scale.

* To whom correspondence should be addressed. E-mail: Oleg.Borodin@utah.edu.
† Department of Materials Science & Engineering, University of Utah.
‡ Department of Chemical Engineering, University of Utah.
§ Department of Chemistry, U.S. Naval Academy.

10.1021/jp061930t CCC: $33.50
Published on Web 08/01/2006

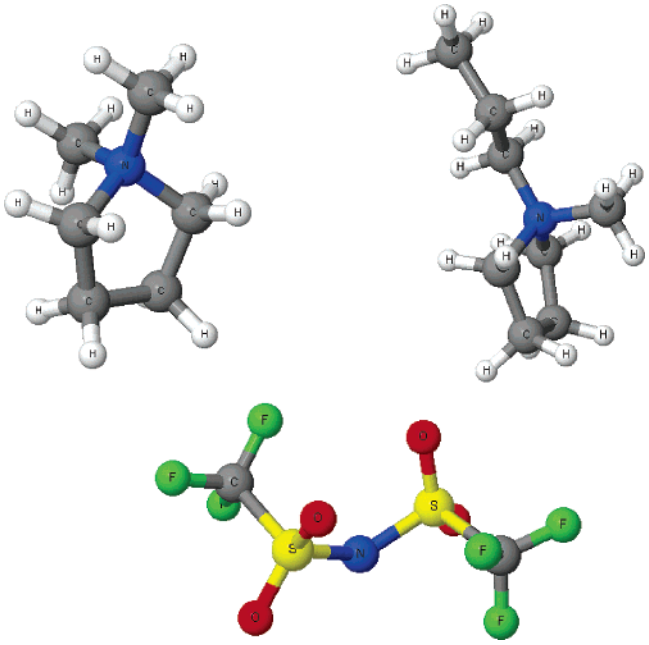

Figure 1. $mmpy^+$, $mppy^+$, and $TFSI^-$ ions.

In this contribution, we examine the Li^+ cation environment in the LiTFSI doped ILs followed by investigation of ion transport with focus on the Li^+ transport mechanism. In the final part of the paper, we compare the Li^+ contribution to ionic conductivity and time-dependent mechanical properties of the investigated LiTFSI doped ILs with those for the poly(ethylene oxide) (PEO)/LiTFSI polymer electrolyte and ethylene carbonate (EC).

We also report conductivity measurements for 0.25 LiTFSI−0.75 $mmpy^+TFSI^-$ and 0.25 LiTFSI−0.75 $mmpy^+TFSI^-$ that were partially reported elsewhere[12,11] together with the details on sample preparation and measurement methodology.

Molecular Dynamics Simulation Methodology. For a detailed description of the simulation methodology employed in the study of the LiTFSI doped ILs, the reader is referred our previous paper detailing simulations of pure ILs.[6] Briefly, the 0.25 LiTFSI−0.75 $mppy^+TFSI^-$ IL consisted of 25 Li^+, 75 $mppy^+$, and 100 $TFSI^-$ ions, while the 0.25 LiTFSI−0.75 $mmpy^+TFSI^-$ IL consisted of 40 Li^+, 120 $mmpy^+$, and 160 $TFSI^-$ ions. The systems were created with an initial periodic cell (box) size of ∼90−120 Å. The cell was shrunk in the MD simulations using a Brownian dynamics algorithm[14] over a period of 0.8 ns at 500 K to yield estimated liquid densities, with subsequent equilibration in the NPT ensemble for 0.6 ns at 500 K. The temperature was then dropped to 393 K, and the systems were equilibrated for 0.9 ns. The NPT runs were used to obtain equilibrium cell sizes corresponding to 1 atm pressure, which were used in the subsequent runs in NVT ensembles as summarized in Table 1. Starting configurations of the electrolytes at 500, 333, and 303 K were taken from configurations of the corresponding electrolytes at 393 K after 1.5 ns NVT runs and reequilibrated for 0.3 ns before the NPT runs reported in Table 1. The slightly negative average pressures for the NVT runs indicates that the density of the IL continued to increase in the NVT runs after the NPT runs used to determine the equilibrium cell size. Negative pressures of this magnitude are expected to have little influence on the structural properties and only a minor influence on the transport properties of the ILs reported in this paper. The equilibrium simulation cell linear sizes were from 35 to 41 Å. Coordinates were stored every 1 ps, while the stress tensor was stored every 8 or 12 fs.

We also performed simulations of 0.25 LiTFSI−0.75 $mppy^+TFSI^-$ and 0.25LiTFSI-0.75 $mmpy^+TFSI^-$ at 393 K with additional interactions between Li^+ and O^{TFSI-} atoms given by

$$U^{add}(r) = -A \exp[-B^*(r - r_0)^2] \quad (1)$$

where r is the distance between Li^+ and O^{TFSI-}, $A = 50$ kcal/mol, $B = 50$ Å^{-2}, and $r_0 = 1.92$ Å. The purpose of this function is to increase the interactions between Li^+ and $TFSI^-$ thus forcing Li^+ to move with its coordinate anions while keeping the structure of the coordination shells unchanged. Finally, two additional MD simulations were performed on the 0.25 LiTFSI−0.75 $mppy^+TFSI^-$ IL at 393 K. In the first simulation, the atomic polarizability of O^{TFSI-} and N^{TFSI-} was set to zero to gain insight into how polarization of the large $TFSI^-$ anion influences the Li^+ cation environment. In the second simulation, a different initial configuration was used to ensure that results do not depend on initial configuration, specifically, all Li^+ cations were separated from each other by at least 5 Å to break up all $TFSI^-$-bridged $Li^+\cdots Li^+$ close (<5 Å) coordinations.

Thermodynamic and Structural Properties of LiTFSI Doped Ionic Liquids. The density of each LiTFSI doped IL at each temperature simulated is given in Table 1. Doping with 0.25 mole fraction LiTFSI increases the density of the $mppy^+TFSI^-$ IL by about 5% compared with pure $mppy^+TFSI^-$ obtained from our previous simulations. MD simulations yield densities of 0.25 LiTFSI−0.75 $mppy^+TFSI^-$ within about 2% of available experimental values.[12] The density of the neat $mppy^+TFSI^-$ IL was predicted in our previous simulations to be within about 1% of experiment at the same temperatures. A similar quality of density predictions for the same force field was observed in our simulations of concentrated oligoethers and carbonates doped with LiTFSI[8] indicating that the force field consistently predicts a density in excellent agreement with experiment.

We began analysis of the structural properties of the LiTFSI doped ILs by calculating various radial distribution functions (RDFs). The Li^+-O^{TFSI-}, Li^+-Li^+, and Li^+-N^{mppy+} RDFs for LiTFSI doped IL are shown in Figure 2. As observed in our

TABLE 1: Properties of 0.25 Li^+TFSI^-−0.75 $mppy^+TFSI^-$ and 0.25 Li^+TFSI^-−0.75 $mmpy^+TFSI^-$ Mixtures from MD Simulations

temp (K)	equilibration run (ns)	production run (ns)	average pressure of NVT runs (atm)	density, MD (kg/m^3)	density experiment (kg/m^3)
		0.25 Li^+TFSI^-−0.75 $mppy^+TFSI^-$			
393	1.2	10.8	−2	1410	
333	0.8	8	−47	1443	1479
303	0.8	13.5	−67	1474	1502
		0.25 Li^+TFSI^-−0.75 $mmpy^+TFSI^-$			
500	0.8	2.3	1	1351	
393	1.0	7.5	34	1465	
333	0.8	7.2	−29	1520	

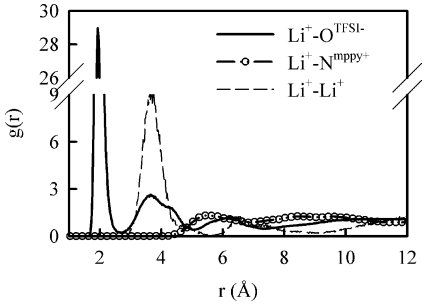

Figure 2. Radial distribution functions in 0.25 $Li^{+}TFSI^{-}$−0.75 $mppyLi^{+}TFSI^{-}$ at 303 K.

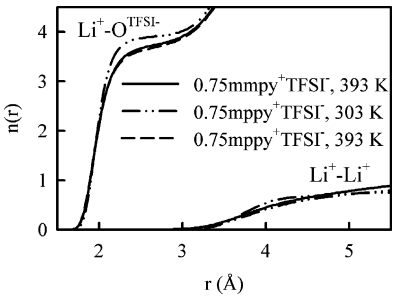

Figure 3. Number of O^{TFSI-} and Li^{+} coordinating a Li^{+} cation within distance *r*.

previous simulations of nonionic polyether[10] and carbonate solutions[9] doped with LiTFSI, an Li^{+} cation is most closely approached by the O^{TFSI-} atoms with the position of the $Li^{+}-O^{TFSI-}$ RDF first peak at 1.92 Å with a peak magnitude of ∼29. The second peak of the $Li^{+}-O^{TFSI-}$ RDF is due to correlations between the Li^{+} cations and other O^{TFSI-} from the same $TFSI^{-}$ anions that contributes to the first peak of the $Li^{+}-O^{TFSI-}$ RDF. Figure 3 shows the running coordination number for the Li^{+} cation. Defining the $Li^{+}-O^{TFSI-}$ first coordination shell by an $r(Li^{+}-O^{TFSI-}) < 2.8$ Å criteria, we find that the Li^{+} cations are coordinated by 3.8 O^{TFSI-} atoms at 393 K and 3.9 O^{TFSI-} atoms at 303 K. As expected, due to the large Coulombic (electrostatic) repulsion between cations, the $mppy^{+}$ cation is separated from the Li^{+} cation by more than 5 Å and is not strongly correlated with the Li^{+} position. Interestingly, the $Li^{+}-Li^{+}$ RDF has a strong peak at 3.7 Å indicating the existence of strong correlations between these cations. The running $Li^{+}-Li^{+}$ coordination number, shown in Figure 3, indicates that each Li^{+} cation has 0.7−0.8 other Li^{+} cations located within 5 Å. Note, that the Li^{+} environment is essentially the same in doped LiTFSI $mmpy^{+}TFSI^{-}$ and $mppy^{+}TFSI^{-}$ ILs.

Figure 4 illustrates two representative configurations of the first coordination shell of the Li^{+} cation. In both configurations, an Li^{+} cation is coordinated by four O^{TFSI-}. We find the probability that a single $TFSI^{-}$ anion will contribute a second oxygen atom the coordination shell of the same Li^{+} cation to be less than 5%. These Li^{+} coordinations are similar to results of X-ray powder diffraction experiments[15] of LiTFSI crystals, in which Li^{+} was found to be tetrahedrally coordinated by four oxygens from four neighboring anions. Figure 4b presents an interesting case, in which a Li^{+} has another Li^{+} situated less than 5 Å away. At 393 K, approximately 65% of the Li^{+} cations form such complexes. The Li^{+} cations are strongly coordinated by sharing up to three $TFSI^{-}$ molecules, that is, they are connected via up to three $Li^{+}\cdots O{=}S{=}O\cdots Li^{+}$ ionic bonds. This type of binding is stabilized via polarization interactions. The presence of two Li^{+} cations on the same side of a $TFSI^{-}$ anion (i.e., coordinated to the same SO_2 group) results in a larger induced dipole moment for a $TFSI^{-}$ anion stabilizing complexes

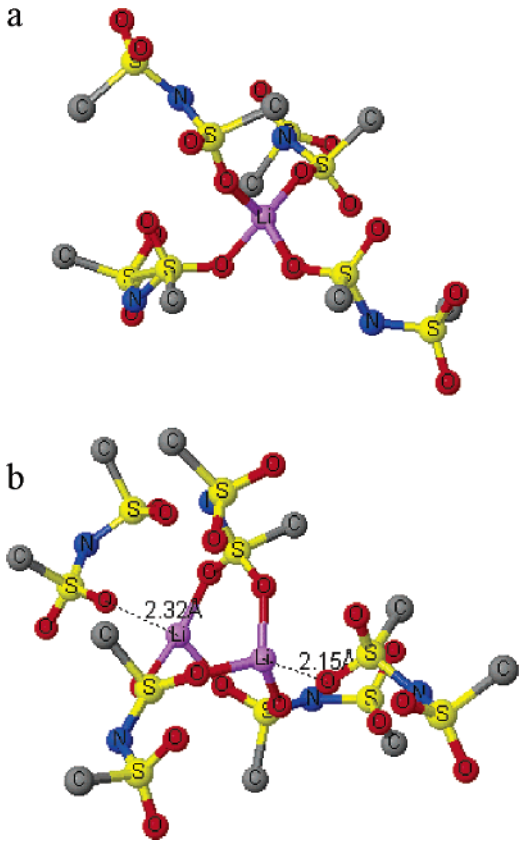

Figure 4. Two representative structures of the Li^{+} first coordination shell. Fluorine atoms of the $TFSI^{-}$ anions are not shown for clarity.

such as the one shown in Figure 4b. To further investigate the importance of the $TFSI^{-}$ polarization on the formation of the $Li^{+}\cdots O{=}S{=}O\cdots Li^{+}$ complexes, we performed an MD simulation of the 0.25 LiTFSI−0.75 $mppy^{+}TFSI^{-}$ mixture at 393 K with the atomic polarizability of O^{TFSI-} and N^{TFSI-} set to zero. These simulations yielded a probability of Li^{+} cations participating in $Li^{+}\cdots O{=}S{=}O\cdots Li^{+}$ complexes of less than 13%, as compared with the 65% found in simulations with the original (unaltered) force field supporting the importance of polarization interactions for formation of the $Li^{+}\cdots O{=}S{=}O\cdots Li^{+}$ complexes. Note, that qualitatively similar $Li^{+}\cdots O{=}S{=}O\cdots Li^{+}$ clustering was also found in our simulations of EC doped with LiTFSI.[9]

The Li^{+} clusters such as those shown in Figure 4b are long-lived, especially at lower temperatures. We quantified the lifetime of the $Li^{+}\cdots O{=}S{=}O\cdots Li^{+}$ complexes by measuring the lifetime autocorrelation function (ACF) $P(t - t_0)$, which gives the probability that the $Li^{+}\cdots O{=}S{=}O\cdots Li^{+}$ complex existing at time t_0 will exist at time t. It is formally defined as

$$P_{Li^{+}-Li^{+}}(t) = \frac{\langle H_{ij}(t)H_{ij}(0)\rangle}{\langle H_{ij}(0)H_{ij}(0)\rangle} \qquad (2)$$

where $H_{ij}(t)$ is 1 if Li^{+} cations i and j are within 5 Å and zero otherwise, $\langle\,\rangle$ denotes average over all time origins and pairs of Li^{+} cations and t_0 set to 0. We assumed that the $Li^{+}\cdots O{=}S{=}O\cdots Li^{+}$ complex exists if the $Li^{+}\cdots Li^{+}$ distance is less than 5 Å corresponding to the minima after the first peak of the $Li^{+}-Li^{+}$ RDF shown in Figure 2.

The $P_{Li^{+}-Li^{+}}(t)$ for the 0.25 LiTFSI−0.75 $mppy^{+}TFSI^{-}$ mixture at three temperatures is shown in Figure 5. At 393 K, the $Li^{+}\cdots Li^{+}$ complex lifetime ACF for 0.25 LiTFSI−0.75 $mppy^{+}TFSI^{-}$ is given by the time scale where $P_{Li^{+}-Li^{+}}(t)$ decays

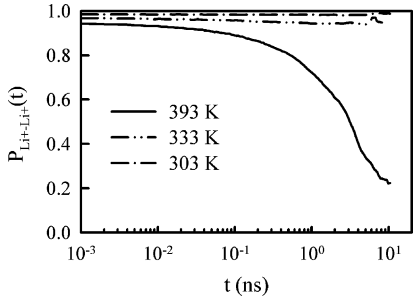

Figure 5. Residence time distribution for Li^+-Li^+ coordination for 0.25 LiTFSI−0.75 $mppy^+TFSI^-$.

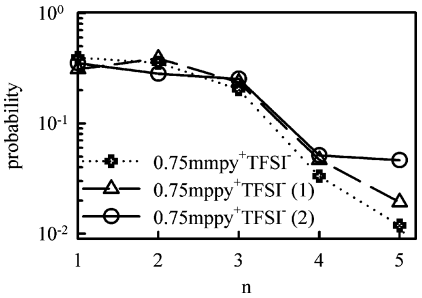

Figure 6. Probability of an Li^+ cation to be a part of the Li^+_n cluster. A Li^+ cation is considered to be part of a cluster if it has another Li^+ from the same cluster within 5 Å. From here on, we use a shorthand notation of 0.75 $mppy^+TFSI^-$ for 0.25 Li^+TFSI^-−0.75 $mppy^+TFSI^-$ and 0.75 $mmpy^+TFSI^-$ for the 0.25 Li^+TFSI^-−0.75 $mmpy^+TFSI^-$ electrolytes to fit it to the plot area. The results for two simulations (1 and 2) for 0.75 $mppy^+TFSI^-$ corresponding to different initial conditions are shown.

to 0.27 ($\approx e^{-1}$). It is about 7.1 ns, indicating slow dissociation-association of the $Li^+\cdots O{=}S{=}O\cdots Li^+$ complexes compared with the average lifetime of the $O(TFSI^-)\cdots Li^+$ coordinations of 1.5 ns at this temperature. At 333 and 303 K, however, $P_{Li^+-Li^+}(t)$ exhibited only a slight decay on the time scale of our simulations (∼10 ns), suggesting that the LiTFSI doped ILs at 303 and 333 K are not well-equilibrated. Similar results were obtained for the 0.25 LiTFSI−0.75 $mmpy^+TFSI^-$ IL.

Further examination of the $Li^+\cdots Li^+$ aggregation behavior revealed the existence of not only lithiums pairs ($Li^+\cdots O{=}S{=}O\cdots Li^+$) but also larger $Li^+\cdots(Li^+\cdots Li^+)_n$ clusters, where each Li^+ is connected to its neighbor via the O=S=O part of $TFSI^-$ anions. The probability for an Li^+ cation to participate in an Li^+_n cluster is shown in Figure 6 for both ILs at 393 K. To further ensure that the equilibrium probability is achieved in our simulations that are only slightly longer than one characteristic time for the $Li^+\cdots O{=}S{=}O\cdots Li^+$ complex form/dissolve, we have performed the second simulation of 0.25 LiTFSI−0.75 $mmpy^+TFSI^-$ with no $Li^+\cdots O{=}S{=}O\cdots Li^+$ complexes in the initial configuration (marked as (2) in Figure 6). The Li^+ cluster distribution is similar for the two simulations with quite different initial conditions confirming that the equilibrium distribution is achieved in simulations. The probability distribution in Figure 6 is similar for $mppy^+TFSI^-$ and $mmpy^+TFSI^-$ ILs doped with LiTFSI.

Finally, we would like to note that simulations of 0.25 Li^+-$TFSI^-$−0.75 $mmpy^+TFSI^-$ at 500 K yielded a fraction of Li^+ not participating in $Li^+\cdots O{=}S{=}O\cdots Li^+$ complexes of 46% compared with 35% at 393 K. Thus, the temperature dependence of the $(Li^+\cdots Li^+)_n$ aggregation is weak with a tendency for greater clustering at lower temperature.

Transport Properties of LiTFSI Doped Ionic Liquids. The self-diffusion coefficient D_i of species i is calculated using the Einstein relation

$$D_i = \lim_{t\to\infty} D_i^{app}(t) = \lim_{t\to\infty} \frac{\langle MSD_i(t)\rangle}{6t} \quad (3)$$

where $MSD_i(t)$ is the mean-square displacement of the center of mass of a molecule of species i during time t, $\langle\ \rangle$ denotes an ensemble average, and $D_i^{app}(t)$ is the time-dependent apparent diffusion coefficient. $\langle MSD_{Li^+}(t)\rangle$ values for the 0.25 LiTFSI−0.75 $mppy^+TFSI^-$ IL are shown in Figure 7. The Li^+ motion is subdiffusive (slope is less than one on the log−log plot) for times less than 1 ns at 393 K, 6 ns at 333 K, and is estimated to be subdiffusive for times less than 33 ns at 303 K.

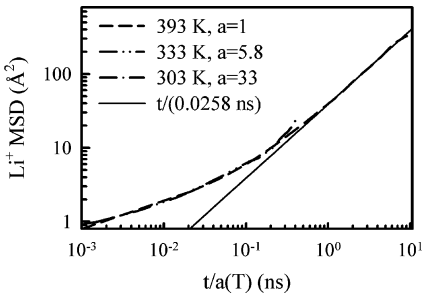

Figure 7. Mean-square displacement (MSD) of Li^+ at various temperatures. Time axis is scaled by the scaling factor $a(T)$.

It is necessary to reach a diffusive regime to accurately extract a self-diffusion coefficient from MD simulations. As the temperature decreases, longer simulations are required to reach the diffusive regime. For example, one needs simulations longer than 35 ns at 303 K for 0.25 LiTFSI−0.75 $mppy^+TFSI^-$. Such simulations are very expensive, especially using the many-body polarizable potentials we employed, thus posing significant difficulties for obtaining the Li^+ self-diffusion coefficient at low temperatures. To estimate the ion self-diffusion coefficient as accurately as possible at low temperatures, we assumed that the $\langle MSD_i(t)\rangle$ values at different temperatures can be superimposed on to each other by scaling the time axis as shown in Figure 7. The self-diffusion coefficients of all ions are determined as

$$D_i(T) = D_i(393\ K)/a_i(T) \quad (4)$$

where D_i(393 K) was obtained utilizing eq 4 at 393 K and $a_i(T)$ is the temperature-dependent time-shift factor obtained by superimposing the $MSD_i(t)$ as shown in Figure 7 for the Li^+ cation.

The self-diffusion coefficients for the ions of the 0.25 LiTFSI−0.75 $mppy^+TFSI^-$ IL from the MD simulations are in good agreement with those from pgf-NMR measurements[12] as seen from Figure 8a. The $mppy^+$ and $TFSI^-$ self-diffusion coefficients are predicted within about 20% of experiment. The Li^+ self-diffusion coefficient is predicted less accurately, with deviations as large as 50%. The $mppy^+$ cations diffuse the fastest, followed by the $TFSI^-$ anions with the Li^+ cations having the lowest self-diffusion coefficient of all ions in the LiTFSI doped IL. The addition of LiTFSI to the $mppy^+TFSI^-$ IL results in a more pronounced decrease of the $TFSI^-$ self-diffusion coefficient than that for $mppy^+$, as shown in Figure 9. The slowing down of ion motion of the $mmpy^+$ and $TFSI^-$ upon addition of the LiTFSI salt scales approximately exponentially with inverse temperature.

The ion self-diffusion coefficients have not been experimentally measured for the 0.25 $LiTFSI^-$−0.75 $mmpy^+TFSI^-$ IL. The predicted ion self-diffusion coefficients for the 0.25

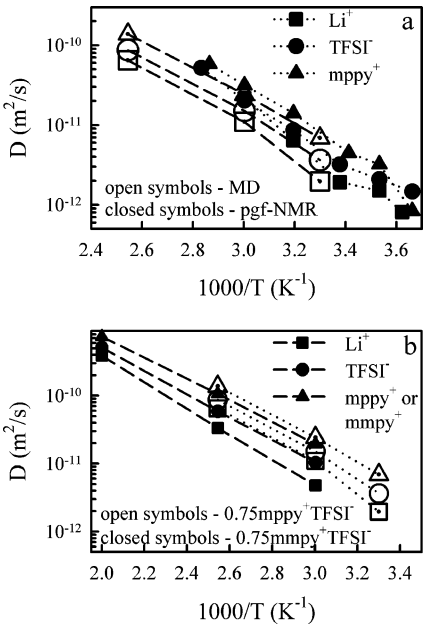

Figure 8. (a) Ion self-diffusion coefficients of 0.25 $Li^{+}TFSI^{-}$−0.75 $mppy^{+}TFSI^{-}$ from MD simulations and pgf-NMR experiments and (b) ion self-diffusion coefficients of 0.25 $Li^{+}TFSI^{-}$−0.75 $mppy^{+}TFSI^{-}$ compared with those for 0.25 $Li^{+}TFSI^{-}$−0.75 $mmpy^{+}TFSI^{-}$ from MD simulations.

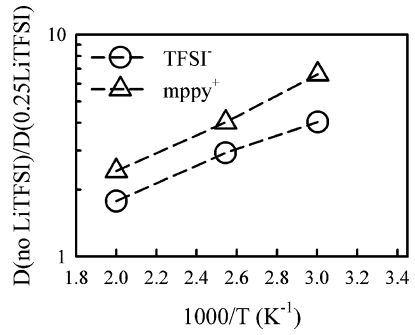

Figure 9. Ratio of ion self-diffusion coefficients of $mppy^{+}TFSI^{-}$ (no $Li^{+}TFSI^{-}$) to those in 0.25 $Li^{+}TFSI^{-}$−0.75 $mppy^{+}TFSI^{-}$.

LiTFSI−0.75 $mmpy^{+}TFSI^{-}$ IL are shown in Figure 8b and are compared with those of the 0.25 LiTFSI−0.75 $mppy^{+}TFSI^{-}$ IL. Ion motion in the 0.25 LiTFSI−0.75 $mmpy^{+}TFSI^{-}$ IL shows a similar temperature dependence to that seen for the 0.25 LiTFSI−0.75 $mppy^{+}TFSI^{-}$ IL. Ion mobility in the $mmpy^{+}$ based IL is about a factor of 2 smaller than that seen in the $mppy^{+}$ based IL possibly because of a lower melting point of the latter.

The ionic conductivity from the MD simulations can be calculated using the Einstein relation

$$\lambda = \lim_{t\to\infty} \lambda^{\mathrm{app}}(t) = \lim_{t\to\infty} \frac{e^2}{6tVk_{\mathrm{B}}T} \sum_{ij}^{N} z_i z_j \langle [\mathbf{R}_i(t) - \mathbf{R}_i(0)][\mathbf{R}j(t) - \mathbf{R}_j(0)] \rangle \quad (5)$$

where e is the electron charge, V is the volume of the simulation box, k_{B} is Boltzmann's constant, T is the temperature, t is time, z_i and z_j are the charges over ions i and j in electrons, $\mathbf{R}_i(t)$ is the displacement of the ion i during time t, the summation is performed over all ions, $\langle\ \rangle$ denotes the ensemble average, and N is the total number of ions in the simulation box, $\lambda^{\mathrm{app}}(t)$ is the apparent time-dependent conductivity. The degree of uncorrelated ion motion (α) is typically measured as the ratio of the collective (total) charge transport (given by λ) to the charge transport due to self-diffusion only (a limit of uncorrelated motion) $\lambda_{\mathrm{uncorr}}$ and is given by

$$\lambda_{\mathrm{uncorr}}{}^{\mathrm{app}}(t) = \frac{e^2}{Vk_{\mathrm{B}}T}(n_{\mathrm{Li}^+}D^{\mathrm{app}}_{\mathrm{Li}^+} + n_{\mathrm{py}^+}D^{\mathrm{app}}_{\mathrm{py}^+} + n_{\mathrm{TFSI}^-}D^{\mathrm{app}}_{\mathrm{TFSI}^-}) = \frac{e^2}{6tVk_{\mathrm{B}}T}\sum_{i}^{N} z_i{}^2\langle[\mathbf{R}_i(t) - \mathbf{R}_i(0)]^2\rangle \quad (6)$$

$$\alpha = \frac{\lambda}{\lambda_{\mathrm{uncorr}}} = \lim_{t\to\infty} \alpha(t) = \lim_{t\to\infty} \frac{\lambda^{\mathrm{app}}(t)}{\lambda^{\mathrm{app}}{}_{\mathrm{uncorr}}(t)} \quad (7)$$

Here, n_i is the number of atoms of type i and py^{+} denote any pyrrolidinium cations ($mppy^{+}$ or $mmpy^{+}$). Thus, $\alpha = 1$ corresponds to uncorrelated ion motion, while $\alpha = 0$ if all of the cations only move together with anions.

The combined pgf-NMR and conductivity measurements[12] on the 0.25 $LiTFS^{-}$−0.75 $mppy^{+}TFSI^{-}$ IL yielded α values around 0.51−0.61 at 293−333 K. The degree of uncorrelated motion from MD simulations is calculated using eqs 5−7 and is shown in Figure 10 for selected temperatures and concentrations. The average values from 0.2 to 1.2 ns for α(t) from Figure 10 are taken as α with estimated uncertainties of ±0.1. MD simulations predict α of 0.6−0.7 for the 0.25 LiTFSI−0.75 $mppy^{+}TFSI^{-}$ IL in good agreement with experiments[12] and 0.4, 0.57, and 0.7 for the 0.25 LiTFSI−0.75 $mmpy^{+}TFSI^{-}$ IL at 333, 393, and 500 K with α slightly increasing with increasing temperature indicative of weaker ion electrostatic interactions relative to thermal motion ($k_{\mathrm{B}}T$) at higher temperatures. Similar values for the degree of uncorrelated motion were found for the pure ILs. The conductivity of ILs from the MD simulations was calculated using self-diffusion coefficients giving $\lambda_{\mathrm{uncorr}}$ (eq 6) and α using eq 7. It is compared with experimental data in Figure 11. Good agreement is observed for 0.25 $Li^{+}TFSI^{-}$−0.75 $mppy^{+}TFSI^{-}$, and good agreement is also seen for predicting the 0.25 $Li^{+}TFSI^{-}$−0.75 $mmpy^{+}TFSI^{-}$ conductivity from simulations.

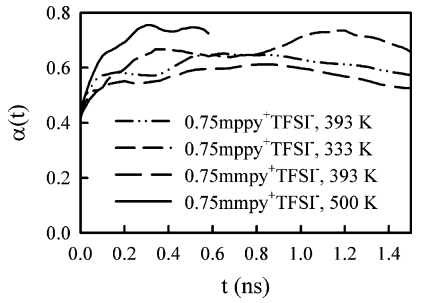

Figure 10. Degree of ion uncorrelated motion α for selected electrolytes.

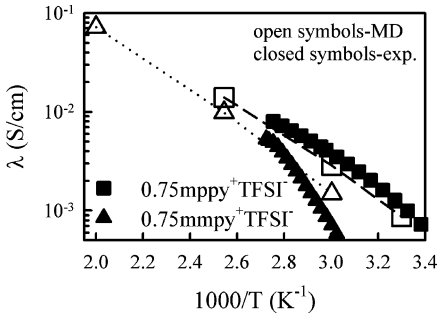

Figure 11. Conductivity of 0.25 $Li^{+}TFSI^{-}$−0.75 mppyTFSI and 0.25 $Li^{+}TFSI^{-}$−0.75 mmpyTFSI from MD simulations and experiments.

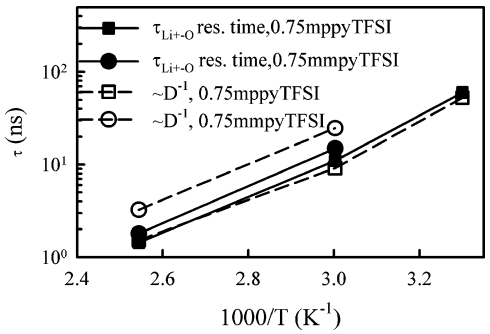

Figure 12. Li^+-O^{TFSI-} residence times and inverse self-diffusion coefficients scaled by an arbitrary constant.

As the next step of our analysis, we focus on understanding the mechanism of the Li^+ cation transport, specifically, we wish to find out if Li^+ cations move primarily with their coordination shells as $Li^+(TFSI^-)_4$ clusters (vehicular mechanism) or by exchanging $TFSI^-$ molecules in their first coordination shell via a structure-diffusion mechanism. One way to quantify the contribution of the vehicular mechanism to the Li^+ transport is to calculate the lifetime of the $Li^+(TFSI^-)_4$ coordinations and how far the $Li^+(TFSI^-)_4$ complex moves before Li^+ exchanges $TFSI^-$ anions in its first coordination shell. The residence time ACF for the Li^+-O^{TFSI-} (P_{Li^+-O}) coordination was calculated using eq 2, with $H_{ij}(t) = 1$ when $r_{Li^+-O^{TFSI-}} < 2.8$ Å and zero otherwise. The residence time was calculated as the integral from zero to infinity to the stretched exponential $\exp[-(t/\tau)^\beta]$ fits to the (P_{Li^+-O}) ACF and is shown in Figure 12. The residence time is on the order of a few nanoseconds and increases approximately exponentially vs inverse temperature. Using self-diffusion coefficient data (Figure 8) and residence times (Figure 12), we estimate that an Li^+ cation on average moves a distance of 1.2−1.6 $TFSI^-$ diameters (diameter is defined as two radii of gyration) before it exchanges a $TFSI^-$ anion in its first coordination shell. These numbers suggest that an Li^+ cation does not diffuse together with its first coordination shell of anions for long distances. In other words, there is a significant contribution to the Li^+ transport mechanism from the structure-diffusion in which Li^+ cations move by exchanging $TFSI^-$ anions.

MD simulations give us the unique ability to estimate the structure diffusion contribution to the Li^+ diffusion coefficient by performing simulations in which we add an additional function (see eq 1) to dramatically slow the exchange of $TFSI^-$ anions in the Li^+ first coordination shell during the simulations, while preserving the structure of the first Li^+ coordination shell. Indeed, the addition of the Li^+-O^{TFSI-} function (eq 1) to the force field does not shift the first peak of the Li^+-O^{TFSI-} position in the MD simulations but does increase its magnitude from 29 to 90. The number of O^{TFSI-} in the Li^+ first coordination shell is 4, which is essentially the same as that in simulations without this additional function. However, increasing the Li^+-O^{TFSI-} interactions results in an increase of the Li^+-O^{TFSI-} residence times by a factor of 12 and 5 for the 0.25 LiTFSI−0.75 $mppy^+TFSI^-$ and 0.25 LiTFSI−0.75 $mmpy^+TFSI^-$ ILs, respectively, as shown in Table 2. With the modified potential, the $TFSI^-$ molecules in the Li^+ first coordination shell are essentially moving together with the Li^+ cations on the scale of multiple solvent diameters.

The artificially increased Li^+-O^{TFSI-} residence times essentially eliminate the structure-diffusion mechanism and lead to a dramatic slowing down of the Li^+ self-diffusion coefficient. As shown in Table 2, the Li^+ diffusion coefficient in the modified ILs is only about 30% of that for the unmodified ILs. Hence, we estimate that the structure diffusion accounts for about 70% of the total diffusion and vehicular contribution is 30%. The diffusion coefficient of the $TFSI^-$ anions is reduced by a factor of 1.6−1.7 because many of them are strongly coordinated by the slower diffusing Li^+ cations. However, the $mmpy^+$ and $mppy^+$ cations that only weakly interact with the Li^+ cations (i.e., do not form part of the first coordination shell of any Li^+ cations) are not slowed by the stronger Li^+-TFSI^- interactions, as shown in Table 2. The temperature dependence of the Li^+-O^{TFSI-} residence times is compared with that for the characteristic time scale for the Li^+ translational diffusion in Figure 12. Similar temperature dependence of these two processes indicates that the Li^+-solvent exchange contribution to the overall Li^+ transport is present at all temperatures to approximately the same extent.

Finally, we note that long-lived Li^+_n pairs (Figure 4b) and clusters have a lower diffusion coefficient compared with that for Li^+ not participating in Li^+_n clusters (Figure 4a) with the difference being most pronounced at lower temperature.

Comparison of Li^+ Transport in ILs with That in Polymer and Liquid Electrolytes. High conductivities of ILs shown in Figure 11 do not reflect their ability to conduct Li^+—one of the most crucial properties for use in lithium batteries. The conductivity due to Li^+ cation transport, denoted as λ^{Li+} is approximated using

$$\lambda^{Li+} = \frac{n_{Li^+}D_{Li^+}}{n_{Li^+}D_{Li^+} + n_{py^+}D_{py^+} + n_{TFSI^-}D_{TFSI^-}}\lambda \qquad (8)$$

where n_i is the number of atoms of type i and py^+ denotes any pyrrolidinium cations ($mppy^+$ or $mmpy^+$). This equation is valid where no ion correlations are present, but we think that it is justifiable to use it here to obtain a rough estimate of λ^{Li+} for ILs, polymer electrolyte (PEO/LiTFSI), and liquid electrolyte (EC/LiTFSI) because the degree of ion uncorrelated motion is rather high, >0.5 for ILs investigated here, >0.88 for PEO/LiTFSI, and >0.5 for EC/LiTFSI.

The conductivity due to Li^+ cation transport (λ^{Li+}) is shown in Figure 13 for ILs and PEO/LiTFSI and EC/LiTFSI from our previous studies.[9,10] Despite liquidlike conductivities of ILs shown in Figure 11, conductivity due to Li^+ cation transport in ILs is dramatically lower than conductivity due to Li^+ cation transport in liquid electrolytes (EC/LiTFSI). In fact, ILs are closer to polymer electrolytes than to liquid electrolytes when it comes to λ^{Li+}. For example, the 0.25 LiTFSI−0.75 $mmpy^+TFSI^-$ has a similar λ^{Li+} to that of PEO/LiTFSI, while 0.25 LiTFSI−0.75 $mmpy^+TFSI^-$ IL has λ^{Li+} 2−3 times higher

TABLE 2: Ratio of Ion Self-diffusion Coefficients and Li^+-O^{TFSI-} Residence Times of 0.25 Li^+TFSI^-−0.75 $mppy^+TFSI^-$ and 0.25 Li^+TFSI^-−0.75 $mmpy^+TFSI^-$ Electrolytes at 393 K for Simulations with the Original Force Field and the Force Field with Additional Li^+-O^{TFSI-} Function (eq 1)

	ratio of properties from simulations with increased Li^+-O^{TFSI-} interactions to those from simulation with the original force field			
electrolyte	$\tau_{Li^+-O^{TFSI-}}$ (ns)	D^{mppy+} or D^{mmpy+}	D^{TFSI-}	D^{Li+}
0.25 Li^+TFSI^-−0.75 $mppy^+TFSI^-$	16.9(ns)/1.44(ns) = 11.7	1/1.15	1/1.6	1/3.2
0.25 Li^+TFSI^-−0.75 $mmpy^+TFSI^-$	9.18(ns)/1.8(ns) = 5.1	1/1.14	1/1.7	1/3.3

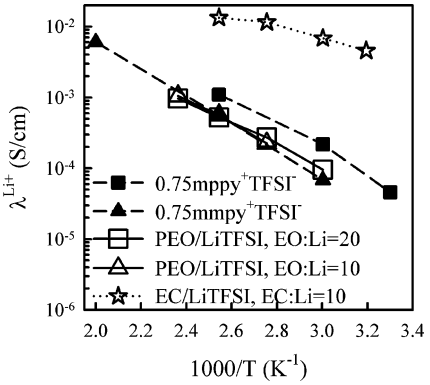

Figure 13. Li^+ contribution to the electrolyte conductivity for ILs and PEO(M_w = 2380)/LiTFSI,[10] EO:Li = 20, and EC/LiTFSI,[9] EC:Li = 10.

over the temperature range shown in Figure 13 and slightly weaker temperature dependence. Such improvements alone (a factor of ~2−3) in λ^{Li+} of ILs over polymer electrolytes are, probably, not enough to advocate the use of LiTFSI doped ILs for battery applications, but combined with improved electrochemical stability, safety, different SEI layer, and so forth, might lead to preference of ILs over polymer electrolytes.

Mechanical Properties. Unlike liquid electrolytes, lithium metal batteries with ILs can be cycled at low currents[17] with no observed dendrites similar to polymer electrolytes.[16,17] This raises the question as to why ILs behave like polymer electrolytes instead of liquid electrolytes when it comes to plating lithium. The different structure of the SEI layer formed in ILs[18] compared with liquid electrolytes is probably responsible for this behavior. It is, however, possible that good mechanical properties of ILs at short times might have an additional contribution to dendrite suppression. Recently, Monroe et al.[19] used the linear elasticity theory to evaluate the impact of the polymer shear modulus and Poisson's ratio on the shapes of periodically roughened lithium/polymer interfaces. They found that the higher the shear modulus of an electrolyte the higher its dendrite suppression ability of the membrane. We calculated the short-time shear moduli of ILs and compared them with those for PEO/LiTFSI and EC to check for correlations between short-time/high-frequency mechanical properties and the ability of electrolyte to suppress dendrite at a certain current.

The shear transverse stress relaxation modulus $G(t)$ can be calculated from MD simulations using the time autocorrelation function of the stress tensor

$$G(t) = \frac{V}{k_B T} \langle P_{\alpha\beta}(t) P_{\alpha\beta}(0) \rangle \qquad (9)$$

where $P_{\alpha\beta}(t)$ is an instantaneous value of the off-diagonal element of the stress tensor at time t, V is the volume of the system, and the brackets denote the averaging over the whole trajectory. The fits to the time-dependent shear modulus $G(t)$ obtained from simulations are shown in Figure 14 for LiTFSI doped ILs, PEO/LiTFSI, and EC. The addition of LiTFSI to mppy^{+}TFSI^{-} increases both the relaxation time for $G(t)$ and glassy modulus given by the short-time (high-frequency) value of shear modulus as shown in Figure 14a. A comparison of $G(t)$ for ILs, PEO/LiTFSI, and EC is shown in Figure 14b. Intriguingly, the subnanosecond shear moduli of ILs and PEO/LiTFSI are very similar. The time-dependent shear modulus for EC is significantly smaller in magnitude and decays much faster than that for ILs and polymer. Thus, we summarize that the mechanical behavior of the simulated ILs is much closer to that

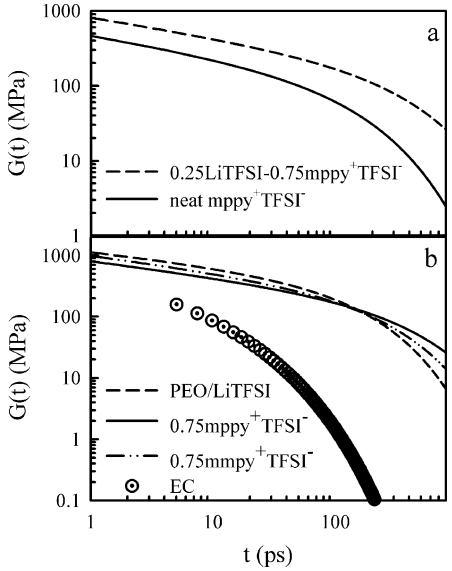

Figure 14. Stretched exponential fits to the time-dependent shear modulus data for ILs doped with LiTFSI at 333 K, PEO(M_w = 2380)/LiTFSI,[10] EO:Li = 20 at 333 K, and EC/LiTFSI,[9] EC:Li = 10 at 313 K.

of polymer electrolytes such as PEO/LiTFSI than regular polar liquid-based electrolytes such as EC/LiTFSI at time scales shorter than Rouse time.

Conclusions

MD simulations were performed on two ILs, mppy^{+}TFSI^{-} and mmpy^{+}TFSI^{-}, doped with Li^{+}TFSI^{-}. The electrolyte conductivity and ion self-diffusion coefficients predicted from the MD simulations with the many-body polarizable force field are in good agreement with experimental data from this and previous work.[12] The Li^+ cations are coordinated by 3.75−3.9 TFSI^{-} anion oxygens, with each TFSI^{-} anion contributing only one oxygen atom to the Li^+ coordination shell. A significant fraction of the Li^+ cations (~60%) have another Li^+ cation within 5 Å, forming aggregates where the Li^+ cations are bridged by Li^+···O═S═O···Li^+ ionic bonds. Such aggregates are very stable at 333 and 303 K on the 10 ns time scale, while at 393 K a lithium joins/leaves an aggregate on a time scale of ~10 ns, on average. Because of the long lifetime of such clusters, the Li^+ cations involved in the Li^+···O═S═O···Li^+ clusters diffuse together with the clusters at a significantly slower rate than the Li^+ cations not coordinated into such clusters.

We have shown that on average Li^+ transport occurs by a combination of two contributions: (a) a dominant contribution (~70% of total) coming from the exchange of TFSI^{-} anions in the Li^+ first coordination shell and outer shells and (b) ~30% of the Li^+ vehicular mechanism (diffusion with the coordination shell).

The Li^+ cation contribution to the electrolyte conductivity (λ^{Li+}) for 0.25 LiTFSI−0.75 mppy^{-}TFSI^{-} was a factor of 2−3 higher than that for 0.25 LiTFSI−0.75 mmpy^{+}TFSI^{-}. The λ^{Li+} value for the later was similar to that for PEO/LiTFSI. ILs doped with LiTFSI had λ^{Li+} values 1−1.5 orders of magnitude lower than EC/LiTFSI for the 303−393 K temperature range indicating low Li^+ transport of ILs compared with liquid electrolytes despite the liquidlike overall conductivities of ILs. Finally, the time-dependent shear modulus of ILs is more similar to that for PEO/LiTFSI polymer electrolyte than conventional EC-based electrolytes.

Acknowledgment. The authors are indebted for a subcontract from Lawrence Berkeley Laboratory BATT Program (#6515401) for financial support. We also would like to thank Stefano Passerini (ENEA, Rome, Italy) for sharing pgf-NMR data.

Appendix

Using atomic virial in conjunctions with the force field, such as the one used in this work that contains high-frequency bends and bonds, results in large periodic oscillations of $G(t)$ due to bonds, bends, and so forth.[20] We obtained smoothed out $G(t)$ by fitting the integral of $G(t)$, that is, $\eta(t)$, see eq a1, with the stretched exponential and subsequently differentiating it to obtain $G(t)$

$$\eta(t) = \int_0^t G(t')\, dt' \qquad \text{(a1)}$$

Note Added after ASAP Publication. This paper was published ASAP on August 1, 2006. Reference 16 was updated with surnames. The revised paper was reposted on August 7, 2006.

References and Notes

(1) Seki, S.; Kobayashi, Y.; Miyashiro, H.; Ohno, Y.; Mita, Y.; Usami, A.; Terada, N.; Watanabe, M. *Electrochem. Solid-State Lett.* **2005**, *8* (11), A577−A578.

(2) Shin, J. H.; Henderson, W. A.; Passerini, S. *Electrochem. Solid-State Lett.* **2005**, *8* (2), A125−A127.

(3) Shin, J. H.; Henderson, W. A.; Passerini, S. *J. Electrochem. Soc.* **2005**, *152* (5), A978−A983.

(4) Adebahr, J.; Seeber, A. J.; MacFarlane, D. R.; Forsyth, M. *J. Appl. Phys.* **2005**, *97* (9).

(5) Adebahr, J.; Forsyth, M.; MacFarlane, D. R. *Electrochim. Acta* **2005**, *50* (19), 3853−3858.

(6) Borodin, O.; Smith, G. D. *J. Phys. Chem. B* **2006**, *110* (23), 11481−11490.

(7) Borodin, O.; Smith, G. D. *J. Phys. Chem. B* **2006**, *110* (12), 6279−6292.

(8) Borodin, O.; Smith, G. D. *J. Phys. Chem. B* **2006**, *110* (12), 6293−6299.

(9) Borodin, O.; Smith, G. D. *J. Phys. Chem. B* **2006**, *110* (10), 4971−4977.

(10) Borodin, O.; Smith, G. D. *Macromolecules* **2006**, *39* (4), 1620−1629.

(11) Henderson, W. A.; Passerini, S. *Chem. Mater.* **2004**, *16* (15), 2881−2885.

(12) Nicotera, I.; Oliviero, C.; Henderson, W. A.; Appetecchi, G. B.; Passerini, S. *J. Phys. Chem. B* **2005**, *109* (48), 22814−22819.

(13) Henderson, W. A. e. a. *Chem. Mat.*, submitted for publication.

(14) Frenkel, D.; Smit, B. *Understanding Molecular Simulation: From Algorithms to Applications*, 2nd ed.; Academic Press: San Diego, CA, 2002.

(15) Nowinski, J. L.; Lightfoot, P.; Bruce, P. G. *J. Mater. Chem.* **1994**, *4*, 1579−1580.

(16) Howlett, P. C.; MacFarlane, D. R.; Hollenkamp, A. F. *Electrochem.Solid-State Lett.* **2004**, *7* (5), A97−A101.

(17) Seki, S.; Kobayashi, Y.; Miyashiro, H.; Ohno, Y.; Usami, A.; Mita, Y.; Kihira, N.; Watanabe, M.; Terada, N. *J. Phys. Chem. B* **2006**, *110* (21), 10228−10230.

(18) Howlett, P. C.; Brack, N.; Hollenkamp, A. F.; Forsyth, M.; MacFarlane, D. R. *J. Electrochem. Soc.* **2006**, *153* (3), A595−A606.

(19) Charles, M.; John, N. *J. Electrochem. Soc.* **2005**, *152* (2), A396−A404.

(20) Byutner, O.; Smith, G. D. *Macromolecules* **2002**, *35* (9), 3769−3771.